Optics Communications 361 (2016) 65–72

Contents lists available at ScienceDirect

Optics Communications

journal homepage: www.elsevier.com/locate/optcom

Photonic crystal with left-handed components

Peter Markoš

Department of Experimental Physics, Faculty of Mathematics, Physics and Informatics, Comenius University in Bratislava, Slovakia

ARTICLE INFO

Article history:
Received 14 July 2015
Received in revised form
21 September 2015
Accepted 18 October 2015

PACS:
42.70.Qs
78.67.Pt

Keywords:
Left-handed materials
Fano resonances
Photonic structures

ABSTRACT

We show that the periodic array of left-handed cylinders possesses a rich spectrum of guided modes when the negative permeability of cylinders equals exactly to minus value of permeability of embedding media. These resonances strongly influence propagation of electromagnetic waves through photonic structures made from left-handed materials. A series of Fano resonances excited by incident wave destroys the band frequency spectrum of square array of left-handed cylinders and increases considerably the absorption of transmitted waves.

1. Introduction

Left-handed (LH) materials which possess, in certain frequency interval, simultaneously negative electric permittivity $\varepsilon < 0$ and magnetic permeability $\mu < 0$ exhibit interesting physical and optical properties, not observed in standard dielectrics or metals [1–3]. Although LH materials are not commonly available in nature, they may be prepared in laboratories and used for construction of devices with prescribed optical properties.

Physical and optical properties of LH materials have been studied during last 15 years from two different points of view. The first, microscopic, approach concentrates on the analysis of the design of individual "atoms" from which periodic macroscopic LH structure is constructed. The aim of this research is to optimize the structure of individual "atom" with respect to its resonant response which guarantee required properties of resulting macroscopic material [4–7]. The second, macroscopic, approach considers homogeneous LH medium with negative ε and μ and investigates its physical properties as well as possible application of LH material in various photonic devices. Typical example of these studies is detailed theoretical and numerical investigations of one dimensional layered structures composed from alternating LH and dielectric layers [8–11].

Recently it has been shown that components made from LH materials may strongly influence optical properties of 2D photonic structures and lead to unexpected phenomena, not observable in conventional photonic structures made from dielectric materials. For instance, the square periodic array of cylinders made from LH material can possess a non-standard band frequency spectrum which contains the so-called folded bands [12,13]. Such results motivate further investigation how the application of LH materials influences the functionality of optical composites.

In this paper we discuss another unusual property of LH photonic structures. We consider periodic arrangements of LH cylinders shown in Fig. 1 and calculate numerically the frequency dependence of the transmission coefficient of incident electromagnetic (EM) wave. Instead of regular transmission bands and gaps, typical for spectra of spatially periodic dielectric structures [14,15], we observe, for small frequencies, a series of irregular maxims and minims in the frequency dependence of transmission coefficient. An example of such irregular frequency dependence is shown in Fig. 2(b). We show that physical origin of these irregularities lies in the excitation of high number of leaky eigenmodes of the structure and consequent interference of excited field with incident electromagnetic field [16–18]. Similar resonances were observed previously in dielectric photonic structures [19] and their influence on the optical response has been analyzed in Refs. [20–22]. We found that the spectrum of excited resonances strongly depends on actual values of negative permittivity and permeability and is extremely rich if one of these parameters coincides with the minus value of the corresponding parameter of embedding media.

The paper is organized as follows. In Section 2, we calculate transmission coefficient of perpendicularly incident EM wave propagating across the linear array of cylinders and through slab constructed from finite number of parallel arrays. We identify a

E-mail address: peter.markos@fmph.uniba.sk

http://dx.doi.org/10.1016/j.optcom.2015.10.042
0030-4018/

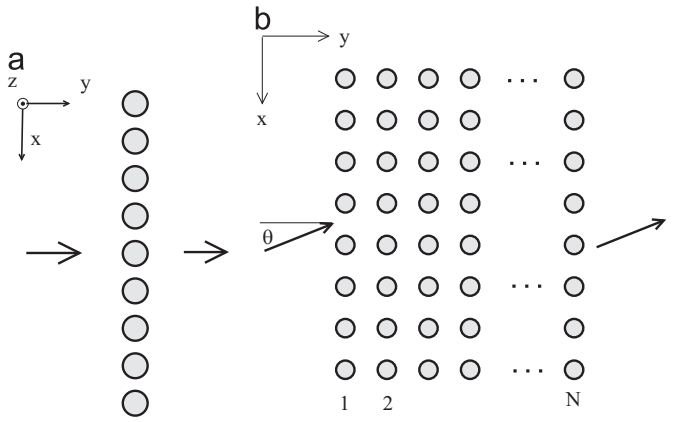

Fig. 1. (a) Periodic linear chain of homogeneous cylinders. Cylinders are parallel to the z-axis, their radius is R, permittivity $\varepsilon = -12$ and permeability $\mu = -1$. The entire structure is periodic in the x direction with spatial period a which is used as a length unit throughout this paper. (b) N parallel chains of cylinders located in planes $y=na$, $0 \le n \le N-1$. The embedding medium is vacuum with permittivity $\varepsilon_1 = 1$ and permeability $\mu_1 = 1$. The incident electromagnetic wave propagating along the y direction with either E_z ($E\|z$) or H_z ($H\|z$) polarization has the wavelength λ and dimensionless frequency $f = a/\lambda$.

series of resonances in the frequency dependence of transmission coefficient. To find their physical interpretation, we analyze the complete spectrum of guided modes of the linear chain of cylinders and show that maxima and minima of the transmission coefficient are associated with Fano resonances excited in the photonic structure by incident EM wave. In Section 3 we study how the electromagnetic response of the structure depends on material parameters: radius of cylinders, magnetic permeability and absorption. Of particular interest is the model with frequency dependent negative permittivity and permeability which also exhibit a series of resonances in the transmission spectra in the frequency interval where either permittivity or permeability approaches the value -1. Since the resonance causes a strong enhancement of electromagnetic field inside the structure, we calculate the absorption of transmitted wave. Conclusion is given in Section 4. Finally, numerical method used for the calculation of the transmissions coefficient is described in Appendices.

2. Linear chain of left-handed cylinders

In this section, we study the response of linear chain of LH cylinders to incident electromagnetic wave. The structure, shown in Fig. 1(a), consists from an infinite periodic chain of cylinders embedded in the vacuum with permittivity $\varepsilon = +1$ and permeability $\mu = +1$. The spatial periodicity of the structure along the x direction, given by distance a between neighboring cylinders, defines the length unit. Cylinders are infinite along the z direction and are made from homogeneous material with relative permittivity $\varepsilon = -12$ and permeability $\mu = -1$.

Incident plane wave with wavelength λ propagates along the y direction. We calculate the transmission and reflection coefficient as a function of dimensionless frequency $f = a/\lambda$. The method is described in Appendix A. Here we only note that electromagnetic field is expanded in series of cylinder functions [23] given by Eqs. (A.2) and (A.3). Expansion on coefficients α and β are calculated from the requirement of continuity of tangential components of electric and magnetic intensity at the boundary of cylinders.

The frequency dependence of the transmission coefficient of the E_z-polarized plane EM wave for both dielectric and LH cylinders is shown in top panels of Fig. 2(a, b). For dielectric cylinders, we identify three deep minima in T which correspond to Fano

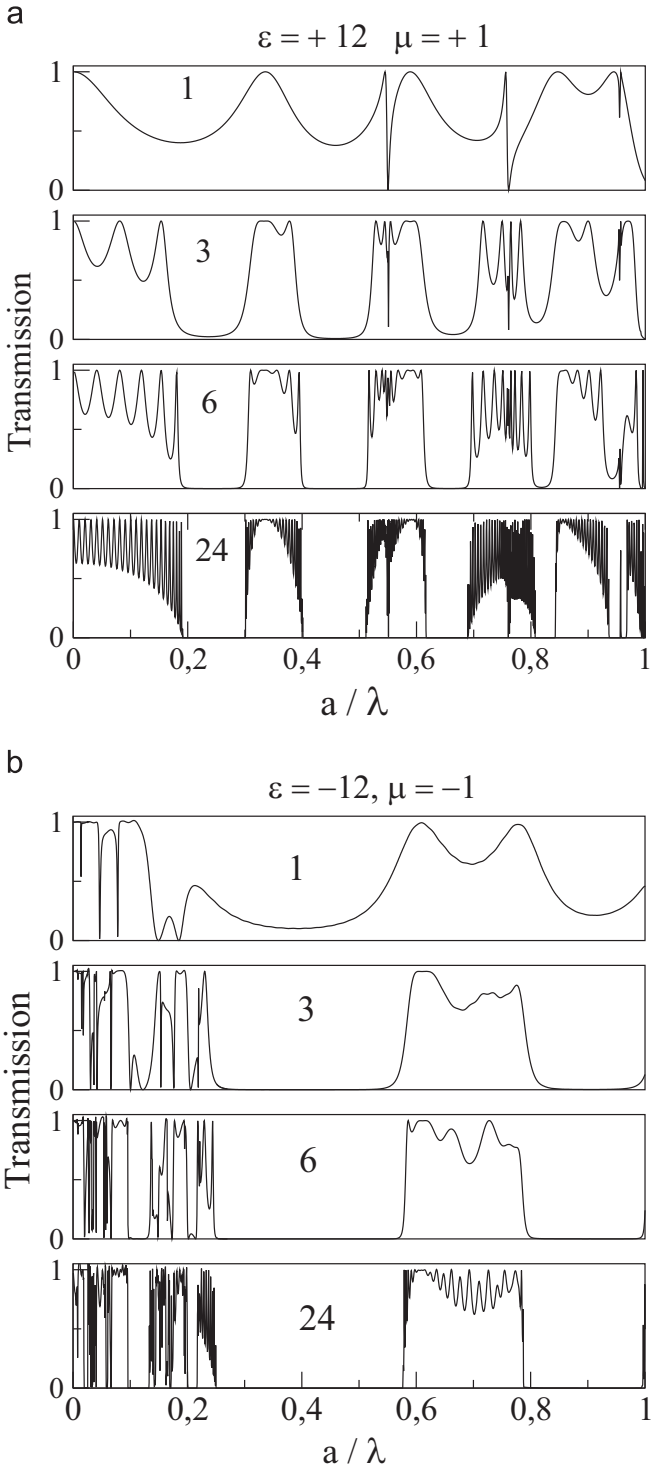

Fig. 2. Transmission spectra for E_z-polarized electromagnetic wave propagating through arrays of (a) dielectric and (b) LH cylinders. The spectra were calculated for $N=1$, 3, 6 and 24 rows of cylinders shown in Fig. 1. The cylinder radius $R = 0.3a$. For dielectric cylinders, the spectrum evolves to transmission bands and gaps when the number of rows increases [29]. In contrast, for LH cylinders, the typical band structure arises only for sufficiently high frequencies, $a/\lambda > 0.2$. For smaller frequencies, the transmission spectrum consists from highly irregular series of maxims and minims.

resonances excited by incident wave [16,22]. Similar resonances were found in the LH structure, but their number is much higher and resonant frequencies are located in the region of small frequencies $a/\lambda < 0.2$. Detailed frequency dependence of the transmission coefficient is given in Fig. 3.

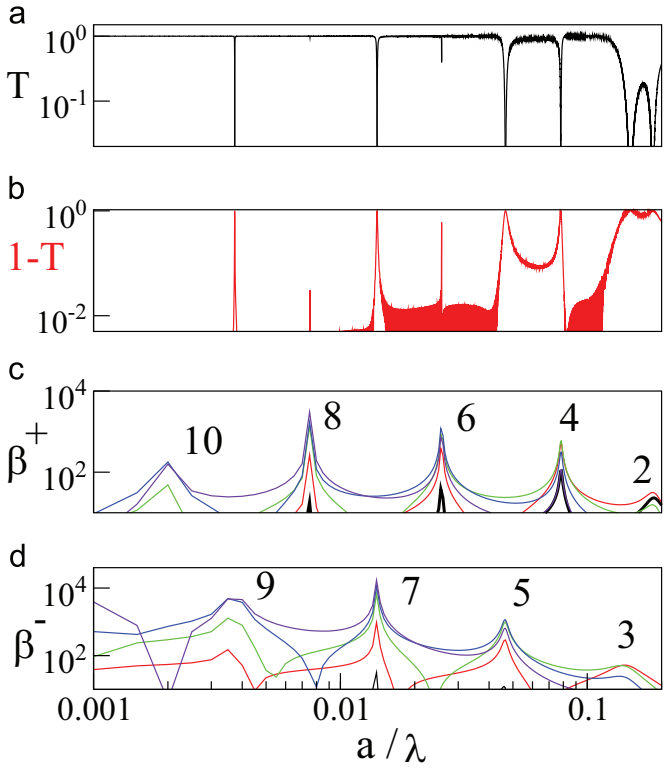

Fig. 3. (a) The frequency dependence of the transmission coefficient of EM wave propagating through linear chain of LH cylinders. Note logarithmic scale on horizontal axis which is identical for all panels. We plot in panel (b) also the difference $1 - T$ which enables us to identify very tiny Fano resonances, not visible in panel (a). Two bottom panels present resonant frequency dependence of coefficients β^+_{2l} (c) and β^-_{2l+1} (d) defined by Eq. (A.3). For numerical reasons, we plot a ratio $\beta^{\pm}_k/H_k(2\pi R/\lambda)$, where H_k is a derivative of the first Hankel function. Since incident field is symmetric with respect to the transformation $x \to -x$, only spatially symmetric resonances are excited [22,24]. The intensity of electric field excited inside cylinders is displayed in Fig. 4.

Lower panels of Fig. 2(a, b) display the transmission coefficient for photonic slabs composed from 3, 6 and 24 rows of cylinders. For dielectric cylinders, Fano resonances develop to narrow Fano bands discussed in detail in Ref. [22]. In contrast, a high number of Fano resonances in the LH structure completely destroy the band structure. Regular transmission band, typical for periodic media, is observed only for higher frequencies $a/\lambda \approx 0.58$.

Following Ref. [22] we expect that the strong irregularities in transmission spectra of linear chain of cylinders are caused by excitation of resonances in the structure. To verify this conjecture, we calculate how coefficients β, which measure the amplitude of excited resonances (Eq. (A.3)), depend on the frequency of incident wave. We found, in agreement with Fig. 3(a), a series of strong resonances, associated with sharp narrow maxims in β (Fig. 3(c, d)). Resonant frequencies coincide with positions of minims in transmission coefficient. Note that owing to even symmetry of perpendicularly incident plane EM wave, only resonances symmetric with respect to transformation $x \to -x$ were excited [24]. Resonant frequencies lie very close to each other (note logarithmic scale of horizontal axis). Comparison of panels (a, b) with (b, c) confirms that each observed transmission minimum corresponds to Fano resonant frequencies.

Data shown in Fig. 3 enable us to identify exponential decrease of resonant frequency f_k when k increases:

$$f_k = f_0 e^{-ck} \tag{1}$$

with constant $c \approx 0.58$.

Fig. 4 displays spatial distribution of electric field e_z inside LH cylinders for nine resonant frequencies $2 \le k \le 10$ identified in Fig. 3. The field concentrated close to the boundary of cylinders. The spatial distribution of field along the boundary reminds us the circular standing waves with the wavelength

$$\Lambda = \frac{2\pi}{k} R. \tag{2}$$

Similar inhomogeneous spatial distribution of EM field has been found also in other photonic systems which contains LH cylinders [27].

2.1. Eigenmodes

Resonances observed in the transmission spectra are given by excitations of eigenmodes of the photonic structures [16]. We calculate the dispersion $f = f(q)$ of guided modes propagating along the linear chain of LH cylinders with wave vector q and frequency $f = a/\lambda$. To find the dispersion curves $f(q)$, we start with two systems of linear equations for coefficients β^+ and β^-, (A.13) and (A.14) with zero right-hand side. Instead of solving these homogeneous systems of equations, we calculate the determinant as a function of frequency [25]. With the use of the Gauss–Jordan elimination method [26] we transform the matrices in the l.h.s. of Eqs. (A.13) and (A.14) into diagonal form and plot the frequency dependence of inverse of obtained diagonal matrix elements. This enables us not only to find the eigenfrequency and lifetime of a given of guided mode but also to identify its order k. Note that method enables us to calculate both guided modes with $f < q$ and leaky modes ($f > q$) with finite lifetime [25].

Fig. 5 presents the dispersion curves $f = f(q)$ of guided modes. For comparison, the spectrum of guided modes of an array of dielectric cylinders is shown in the inset. As expected, the spectrum for left-handed cylinders is more complicated. In contrast to dielectric cylinders [22], the number of guided modes is much higher. The number of modes depends on the model parameters and increases when absolute value of the refractive index increases (data not shown). In agreement with Eq. (1), their eigenfrequencies decrease when the mode index k increases.

Another unexpected property of spectra of guided modes is the existence of "critical value" of the wave vector q_c ($q_c \approx \pi/2a$ in our model) for which no guided mode exists (Fig. 5). Analysis of another left-handed structures with $\mu = -1$ (data not shown) indicates that q_c depends neither on (negative) permittivity nor on the radius of cylinder.

3. Parameters of the model

In this section we investigate how the spectrum of resonant modes depends on the parameters of the model.

3.1. Radius of cylinder

Very narrow resonances in the transmission coefficient for the frequency $a/\lambda < 0.08$ as well as broad minimum of the transmission at $a/\lambda \sim 0.28$ shown in Fig. 6(a) indicate that Fano resonances can be observed already in the linear chain of very tiny ($R = 0.1a$) LH cylinders. The transmission coefficient of photonic slab exhibits a broad gap for small frequencies with a few narrow resonances at small frequencies $a/\lambda \le 0.09$. Broad transmission band, typical for periodic structures, started at $a/\lambda \approx 0.65$.

Fig. 6(b) shows that the frequency dependence of the transmission coefficient is more dramatic when the radius of cylinders increases. For the E_z polarized wave, the frequency dependence of T is highly irregular, indicating the high number of resonances in

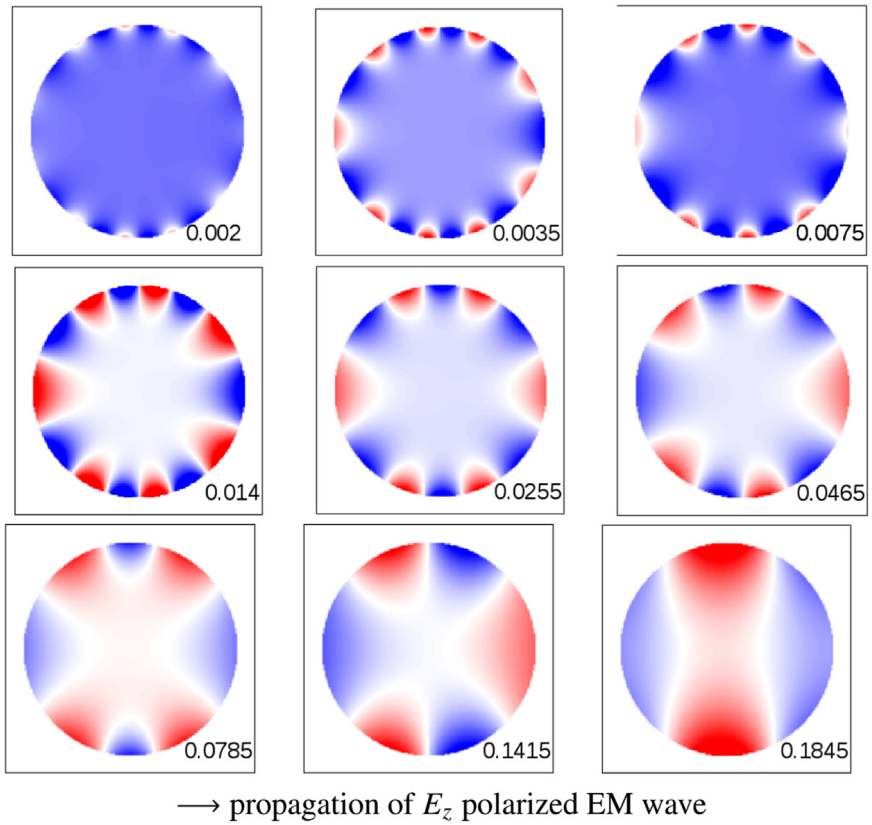

Fig. 4. The spatial distribution of electric intensity e_z inside cylinders arranged in a linear chain for resonances $2 \le k \le 10$. Resonant dimensionless frequencies a/λ, identified in Fig. 3, are given in legends. Index k determines the period of the wave around the cylinder surface in agreement with Eq. (1). The incident e_z polarized electromagnetic wave propagates from left to the right (Fig. 1).

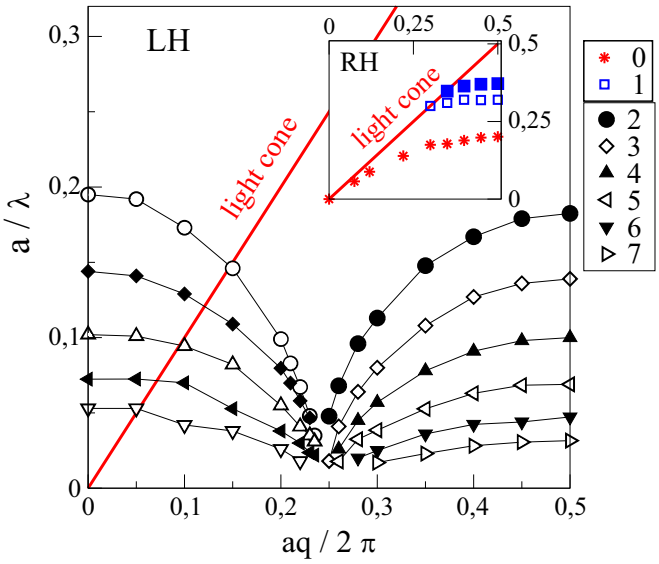

Fig. 5. Spectrum of guided modes $f = a/\lambda = f(q)$ calculated for linear chain of LH cylinders (Eq. (A.13)). Open and full symbols correspond to spatially even and odd modes, respectively. Note that modes change their spatial symmetry when q crosses critical value $q_c \approx \pi/2a$. For comparison with dielectric structures, the inset shows the spectrum for linear chain of dielectric cylinders with permittivity $\varepsilon = +12$ and permeability $\mu = +1$.

the structure. Only for higher frequency, regular transmission band is observed.

Note that in contrast to the E_z waves, the transmission coefficient for the H_z wave typical frequency dependence typical for dielectric photonic crystals independently on the cylinder radius. As we will see later, the absence of Fano resonances is due to big difference in absolute values of the permittivity $\varepsilon = -12$ inside cylinders and permittivity $\varepsilon_1 = +1$ of the embedding medium.

3.2. Permeability

Photonic structures discussed up to now possess LH components with effective permeability $\mu = -1$ equal exactly to minus value of the permeability μ_1 of the embedding media. This coincidence might be responsible for strong resonances of electromagnetic field observed in previous sections. We note that spatial distribution of the EM field with high values of the intensity close to cylinder boundary (Fig. 4) is similar to surface plasmons excited at the planar interface of vacuum and LH media [29] and that the dispersion relation of the E_z polarized surface plasmon wave (with electric field parallel to the interface) is singular when the permeability μ equals to minus value of permeability of embedding media [29,30]. Of course, the analogy is not exact since, in contrast to our resonant states, surface plasmon cannot be excited by incident EM wave.

Fig. 7 shows the transmission coefficients and spectra of coefficients β for linear chain of LH cylinders with permeability slightly below and above the critical value $\mu = -1$. The positions of resonances in frequency spectra are very sensitive to the actual value of μ: for smaller (in absolute value) μ, resonances shift to frequencies $f > 0.1$, while for larger values of permeability they disappear.

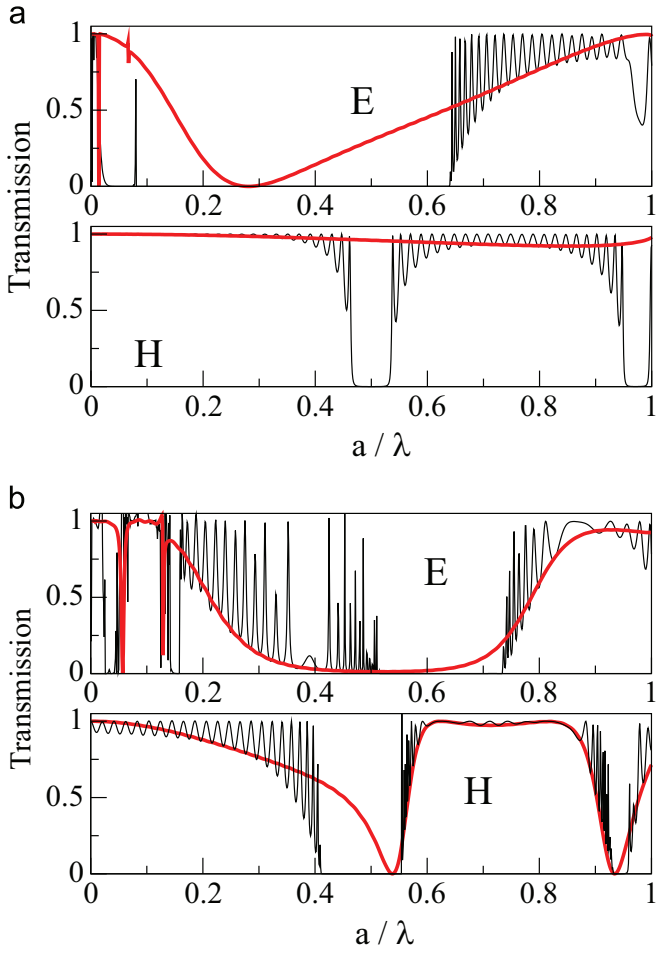

Fig. 6. Transmission coefficient of plane electromagnetic wave propagating across the linear array of LH cylinders (bold red line) and through periodic structure constructed from 24 rows of cylinders (thin black line). The radius of cylinders is $R = 0.1a$ (a) and $R = 0.2a$ (b). Polarization of EM wave is given in panel legends. (For interpretation of the references to color in this figure caption, the reader is referred to the web version of this paper.)

3.3. Dispersive LH materials

Since realistic LH materials are dispersive [1], it is important to generalize our analysis to structures made from dispersive LH materials. We consider LH cylinders with frequency dependent permittivity

$$\varepsilon(f) = 1 - \frac{1}{f^2} \tag{3}$$

and permeability

$$\mu(f) = 1 - 0.4\frac{f^2}{f^2 - f_0^2} \quad (f_0 = 0.4). \tag{4}$$

Transmission coefficient for arrays of such cylinders is shown in Fig. 8 both for the E_z and H_z polarized EM waves.

For small frequency $f < f_0$ the permittivity is negative and permeability is positive. The transmission coefficient exhibits the frequency dependence typical for an array of metallic cylinders [28] with low frequency transmission gap for the E_z polarized wave and regular transmission band for the H_z polarized wave. Irregular frequency dependence for f slightly above $f_0 = 0.4$ is due to the large value of the effective index LH material. More interesting is the transmission coefficient for the E_z polarized wave in the frequency region around $f_e = 0.447$ defined by relation

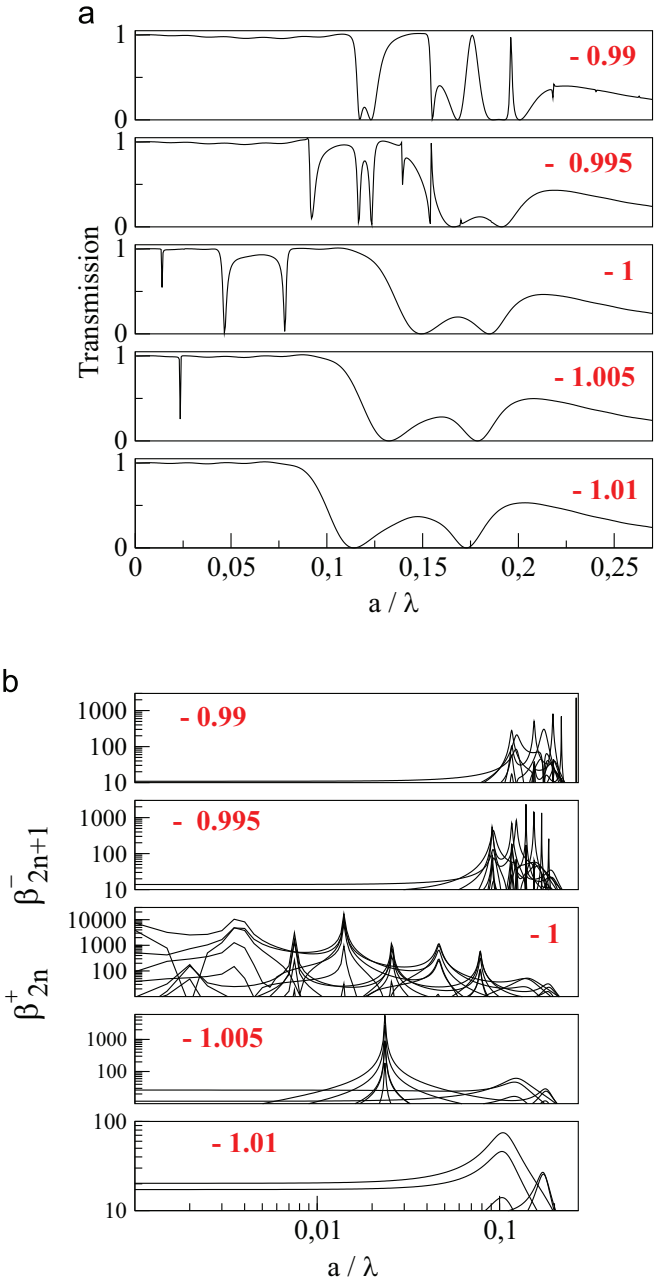

Fig. 7. (a) Transmission coefficient T for linear array of LH cylinders with radius $R = 0.3a$, $\varepsilon = -12$ and various values of magnetic permeability μ (given in legends). (b) Frequency dependence of coefficients β for linear array of cylinders. Note the strong sensitivity of resonant frequencies to small changes of permeability. Cylinders are embedded in vacuum with permeability $\mu_1 = 1$.

$\mu(f_e) = -1$ which exhibits irregular frequency dependence similar to that discussed in Section 2. Similar resonant behavior is observed for the H_z-polarized wave in the vicinity of frequency $f_m = 0.7$, where the permittivity of LH material approaches minus unity.

3.4. Absorption

As discussed in [22], high intensity of EM field inside cylinders may cause strong enhancement of the absorption of transmitted EM wave for frequencies close to resonant Fano frequency. Fig. 9 demonstrates an increase of the absorption in photonic structures with LH cylinders. Absorption is close to unity already for very

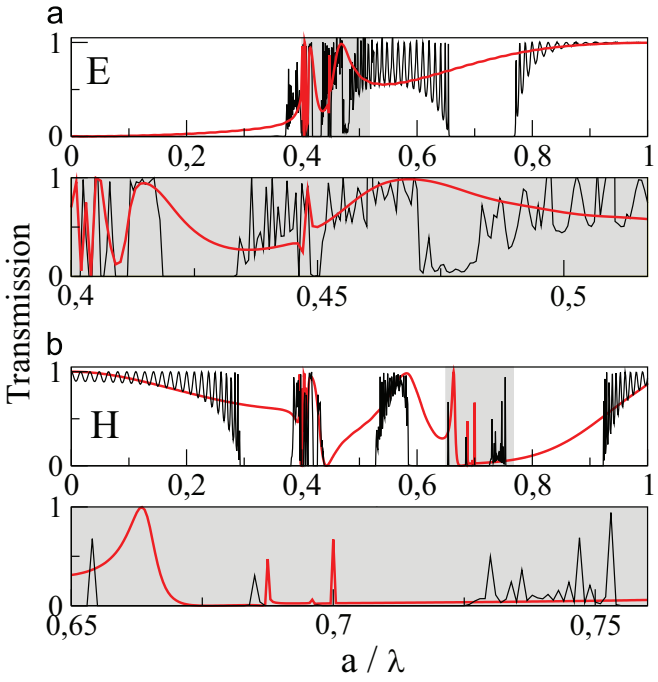

Fig. 8. Transmission coefficient of plane electromagnetic wave propagating through square array of cylinders made from left-handed dispersive medium. The cylinder permittivity and permeability is given by Eqs. (3) and (4), respectively. The permittivity is negative in the whole frequency interval $0 < f < 1$, and permeability is negative when $f_0 < f < f_0/\sqrt{0.6} = 0.516$. (a) E_z polarization (intensity of electric field is parallel to the cylinder axis). The transmission coefficient exhibits irregular frequency dependence in the vicinity of frequency $f_e = a/\lambda_e = 0.447$ where $\mu(f_e) \approx -1$. For the H_z polarized wave (panel (b)), similar irregularities are observed around the frequency $f_m = a/\lambda_m \approx 0.7$, where $\varepsilon(f_m) \approx -1$.

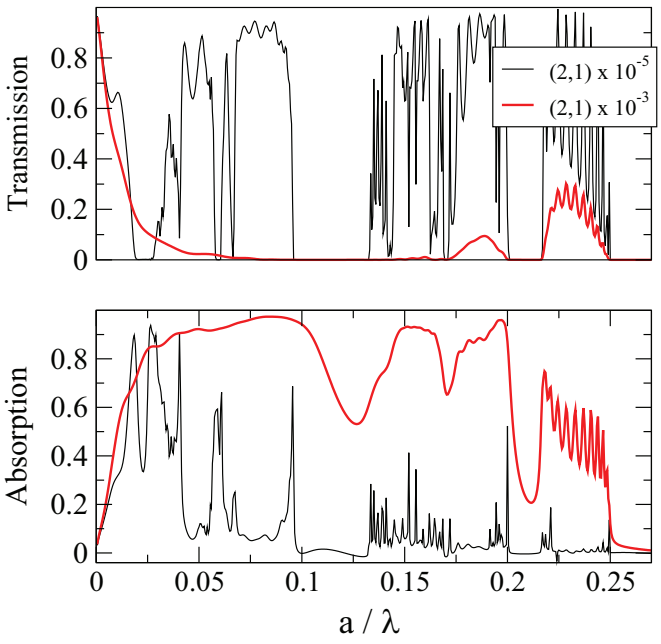

Fig. 9. Transmission coefficient and absorption for the photonic crystal with cylinders made from the left-handed material ($\varepsilon = -12$, $\mu = -1$) and with small imaginary part of permittivity and permeability (given in legend) as a function of the dimensionless frequency $a/\lambda < 0.27$.

small values of imaginary part of permittivity and permeability, Imag ε, $\mu \sim 10^{-3}$. Since Fano resonances lie close to each other, we obtained broad absorption band with absorption coefficient close to unity.

4. Conclusion

We have shown that transmission spectra of photonic structures with LH components might be strongly influenced by Fano resonances excited by incident electromagnetic wave. Fano resonances play an important role especially when the permittivity and/or permeability of the LH material is close to -1. As such values exist in any realistic dispersive LH medium, we expect that irregular resonant behavior, discussed in this paper, might be observed experimentally. However, non-zero imaginary part of permittivity and permeability strongly enhanced absorption losses due to large amplitudes of electromagnetic waves inside cylinders. Therefore, instead of irregular resonant transmission, found numerically in loss-less materials, we expect that a broad absorption band in the resonant frequency region will be measured.

We also found that the spatial distribution of the electromagnetic field inside the cylinders is highly inhomogeneous with strong field enhancement in the narrow region in the vicinity of the boundary of cylinder.

Acknowledgments

This work was supported by the Slovak Research and Development Agency under the Contract no. APVV-0108-11 and by the Agency VEGA under the Contract no. 1/0372/13.

Appendix A. Numerical methods

In this section we describe the numerical method used for the calculation of the transmission of electromagnetic wave with wavelength λ propagating across linear chain of cylinders shown in Fig. 1(a). Owing to the cylinder symmetry, we express electric and magnetic fields in cylindrical coordinates. Consider the E_z-polarized electromagnetic wave, $\vec{E} = (0, 0, e_z)$ (the H_z polarized wave can be treated in the same way). Two non-zero components of the magnetic field, the angular, h_φ, and the radial, h_r, ones can be found with the use of Maxwell equations [31]

$$i\omega\mu h_\varphi(r,\varphi) = -\frac{\partial e_z}{\partial r}, \quad i\omega\mu h_r(r,\varphi) = \frac{1}{r}\frac{\partial e_z}{\partial \varphi}. \tag{A.1}$$

For cylinder centered in $(x, y) = (0, 0)$ we express the electric intensity e_z as a sum of cylinder functions [23]. Inside the cylinder ($r \le R$) we have

$$e_z^{\text{in}}(r,\varphi) = J_0(\nu)\alpha_0^+ + 2\sum_{k=1}\alpha_k^+ J_k(\nu)\cos(k\varphi) + 2i\sum_{=1}\alpha_k^- J_k(\nu)\sin(k\varphi), \tag{A.2}$$

where J_k is Bessel function of integer order, $\nu = 2\pi rn/\lambda$, and $n = \sqrt{\varepsilon\mu}$ is the index of refraction. Coefficients α^+ and α^- determine amplitudes of even ($\propto\cos k\varphi$) and odd ($\propto\sin k\varphi$) cylindrical waves, respectively. In Eq. (A.2), as well in all expressions below, the summation over k is restricted to N_B lowest order cylinder functions ($k \le N_B$).

The electric field outside the cylinder consists from three contributions: the first one is the field scattered on the cylinder itself [23]

$$e_z^0(r,\varphi) = H_0(u)\beta_0^+ + 2\sum_{k=1}\beta_k^+ H_k(u)\cos(k\varphi) + 2i\sum_{k=1}\beta_k^- H_k(u)\sin(k\varphi) \quad (u = 2\pi r/\lambda) \tag{A.3}$$

($r \ge R$). Here, $H_k(z) = J_k(z) + iY_k(z)$ is the first Hankel function

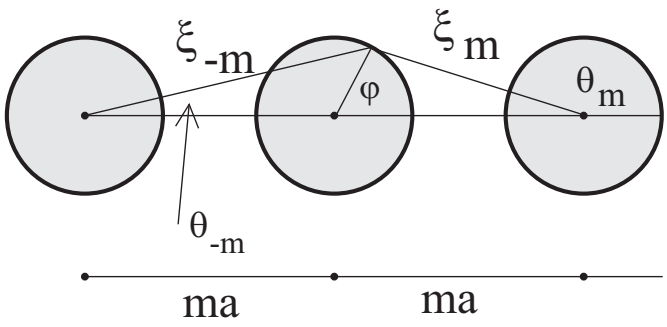

Fig. A1. Parameters used in derivation of Eq. (A.4).

[23,32].

The second contribution to the external fields consists from fields scattered on other cylinders present in the structure. In particular, the contribution of the mth cylinder ($m = \pm 1, \pm 2, \ldots, N_s$) expressed as a function of coordinates associated with its center (Fig. A1) reads

$$e_z^m(\xi_m, \theta_m) = H_0(w_m)\beta_{m0}^+ + 2\sum_{k>0}\beta_{mk}^+ H_k(w_m)\cos(k\theta_m) + 2i\sum_{k>0}\beta_{mk}^- H_k(w_m)\sin(k\theta_m) \quad (w_m = 2\pi\xi_m/\lambda). \tag{A.4}$$

Note that coefficients β_{mk} differs from β_k defined in Eq. (A.3). However, thanks to the periodicity of the structure along the x-axis, we can use Bloch's theorem and express $\beta_{mk}^{\pm}$ of the mth cylinder in terms of coefficients $\beta_k^{\pm}$ as

$$\beta_{mk}^{\pm} = e^{iqma}\beta_k^{\pm} \tag{A.5}$$

where q is the x-component of the wave vector of EM field.

Finally, the third contribution is given by incident electromagnetic wave. For instance, the plane wave incident perpendicularly to the cylinder chain (Fig. 1(b)) can be expressed as a sum of Bessel function [32]

$$e_z^i(r, \varphi) = J_0(u) + 2\sum_{k=1} J_{2k}(u)\cos(2k\varphi) + 2i\sum_{k=1} J_{2k-1}(u)\sin[(2k-1)\varphi]. \tag{A.6}$$

Unknown coefficients α and β defined in Eqs. (A.2)–(A.4) are calculated from the requirement of the continuity of tangential components of electric and magnetic fields at the boundary of each cylinder. Thanks to Eq. (A.5), it is sufficient to formulate the continuity conditions only for the cylinder located at the center of coordinates. Since e_z is parallel to cylinder surface, the requirement of the continuity of electric field is easy to formulate,

$$e_z^{\text{in}}(R^-, \varphi) = e_z^{\text{out}}(R^+, \varphi) = e_z^i(R^+, \varphi) + e_z^0(R^+) + \sum_{n\neq 0} e_z^n(\xi_n, \theta_n). \tag{A.7}$$

The continuity condition for the magnetic field is expressed in more complicated form

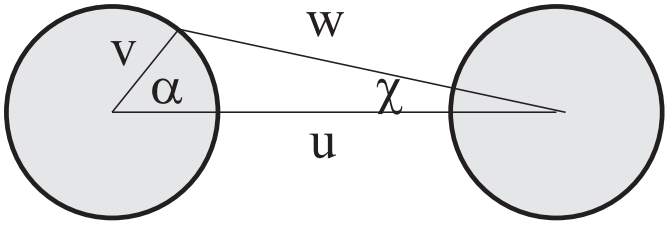

Fig. A2. Parameters used in Gegenbauer's relation, Eqs. (A.9) and (A.10).

$$h_\varphi^{\text{in}}(R^-) = h_{\text{tang}}^{\text{out}} = h_\varphi^i(R^+, \varphi) + h_\varphi^0(R^+, \varphi) + \sum_{n\neq 0}[h_{\theta_n}^n(\xi_n, \theta_n)\cos\alpha_n - h_{r_n}^n(w_n, \theta_n)\sin\alpha_n] \tag{A.8}$$

where the angle $\alpha_n = \theta_n - \varphi$.

Before solving this system of equations, we express all fields in Eq. (A.4) in terms of variables r and φ associated with the cylinder located at the point $x=0$, $y=0$. This can be done with the use of the Gegenbauer formula for cylindrical functions (Fig. A2)

$$H_m(w)e^{\pm im\chi} = \sum_{k=-\infty}^{+\infty} H_{m+k}(u)J_k(v)e^{\pm ik\alpha} \tag{A.9}$$

and their derivative $H_m'(w)$:

$$H_m'(w)e^{\pm im\chi} = \sum_{k=-\infty}^{+\infty} H_{m+k}'(u)J_k(v)e^{\pm ik\alpha} \tag{A.10}$$

[32] . Inserting (A.10) into Eq. (A.4) we express, after some algebra, the fields at the outer boundary of the cylinder in the form

$$e_z^{\text{out}}(R^+, \varphi) = \sum_{k,m=0}\mathbf{B}_{km}\beta_m^+\cos k\varphi + \sum_{k,m=1}\mathbf{C}_{km}\beta_m^-\sin k\varphi \tag{A.11}$$

and

$$h_t^{\text{out}}(R^+, \varphi) = \sum_{k,m=0}\mathbf{B}'_{km}\beta_m^+\cos k\varphi + \sum_{k,m=1}\mathbf{C}'_{km}\beta_m^-\sin k\varphi. \tag{A.12}$$

Explicit expressions for matrices $\mathbf{B}$, $\mathbf{B}'$, $\mathbf{C}$ and $\mathbf{C}'$ are given in Appendix B.

In the next step, we eliminate coefficients α from Eqs. (A.11) and (A.12) and obtain two separate systems of linear equations for coefficients β^+ and β^-:

$$\sum_m\left[\mathbf{B}_{km} - \zeta\frac{\mathcal{J}_k}{\mathcal{J}_k'}\mathbf{B}'_{km}\right]\beta_m^+ = e_k^+ - \zeta\frac{\mathcal{J}_k}{\mathcal{J}_k'}h_k^+, \tag{A.13}$$

$k, m = 0, 1, \ldots, N_B$, and

$$\sum_m\left[\mathbf{C}_{km} - \zeta\frac{\mathcal{J}_k}{\mathcal{J}_k'}\mathbf{C}'_{km}\right]\beta_m^- = e_k^- - \zeta\frac{\mathcal{J}_k}{\mathcal{J}_k'}h_k^-, \tag{A.14}$$

$k, m = 1, \ldots, N_B$. Here, $\mathcal{J}_k = J_k(2\pi nR/\lambda)$ and

$$\zeta = \sqrt{\frac{\mu}{\varepsilon}} \quad (\text{Real } \zeta > 0) \tag{A.15}$$

is the impedance of cylinders. In numerical analysis, we consider the number of cylinders $N_s \leq 20\,000$ and number of modes $N_B \leq 12$.

Transmission coefficient can be calculated as the ratio of the y-component of the Poynting vector $S_x(y_p)$, calculated for any $y_p > r$ to the incident Poynting vector, $S_y{}^i$

$$T = \frac{S_x(y_p)}{S_x^i} \tag{A.16}$$

where

$$S_x(y_p) = \int_{-a/2}^{+a/2} dx e_z(x, y_p)h_x^*(x, y_p) \tag{A.17}$$

and

$$S_x^i = \int_{-a/2}^{+a/2} dx e_z^i(x, y_p)(h_x^i(x, y_p))^*. \tag{A.18}$$

Similarly, reflection coefficient R is given by

$$R = \frac{S_x(y_p)}{S_x^i} \tag{A.19}$$

where

$$S_x(y_p) = \int_{-a/2}^{+a/2} dx (e_z - e_z^i)(h_x - h_x^i)^* \tag{A.20}$$

calculated for $y_p < -r$.

Appendix B. Matrices B and C

With notation $J_k \equiv J_k(u)$ and $\mathcal{H}_k = H_k(u)$, $u = 2\pi R/\lambda$ we express the explicit form of the $(N_B + 1) \times (N_B + 1)$ matrix **B**

$$B_{00} = \mathcal{H}_0 + \sum_{n=1}^{N_s} 2\cos qH_0(un)J_0$$

$$B_{0m} = \sum_{n=1}^{N_s} H_m(un)J_0 \times [(-1)^m e^{iqan} + e^{-iqan}]$$

$$B_{k0} = \sum_{n=1}^{N_s} H_k(un)J_k \times 2[e^{iqan} + (-1)^k e^{-iqan}]$$

$$B_{km} = 2\mathcal{H}_k\delta_{km} + \sum_{n=1}^{N_s} [e^{iqan}(-1)^{m-k} + e^{-iqan}][H_{m-k}(un) + (-1)^k H_{m+k}(un)]J_k \tag{B.1}$$

($k, m = 1, 2, \ldots, N_B$). The $N_B \times N_B$ matrix **C** has a form

$$C_{km} = 2\mathcal{H}_k\delta_{km} + \sum_{n=1}^{N_s} [e^{iqan}(-1)^{m-k} + e^{-iqan}] \times [H_{m-k}(un) - (-1)^k H_{m+k}(un)]J_k \tag{B.2}$$

Matrices $\mathbf{B}'$ and $\mathbf{C}'$ could be obtained from **B** and **C**, respectively, by substitutions

$$J_k \to J_k', \quad \mathcal{H}_k \to \mathcal{H}_k'. \tag{B.3}$$

Appendix C. System with *N* rows of cylinders

If the system consists of N rows of cylinders (the nth row lies in plane $y = (n-1)a$, z), then we have to define N sets of parameters $\beta_{yk}^{\pm}$, each for the nth cylinder along the y direction. The method of calculation remains the same as for the linear chain with $N=1$, but resulting linear relations between coefficients $\beta_{nk}^{\pm}$ are more complicated. In particular, it is not possible to separate coefficients β^+ and β^-. Resulting system of linear equations for coefficients $\beta_{nk}^{\pm}$ is of the size $N \times (2N_B + 1)$. For $N_B = 12$ (typically used in numerical simulations) and $N = 24$ the problem reduces to the solution of 600 linear equations.

References

[1] V.G. Veselago, Sov. Phys. Usp. 10 (1968) 509.
[2] J.B. Pendry, Phys. World 14 (2001) 47;
J.B. Pendry, Contemp. Phys. 45 (2004) 191.
[3] N. Engheta, R.W. Ziolkowski (Eds.), Metamaterials: Physics and Engineering Explorations, J. Wiley & Sons, New York, 2006.
[4] R.A. Shelby, D.R. Smith, S. Schultz, Science 292 (2001) 77.
[5] J.B. Pendry, Phys. Rev. Lett. 85 (2000) 3966.
[6] J.B. Pendry, D. Schurig, D.R. Smith, Science 312 (2006) 1780.
[7] N.I. Landy, S. Sajuyigbe, J.J. Mock, D.R. Smith, W.J. Padilla, Phys. Rev. Lett. 100 (2008) 207402.
[8] J. Li, L. Zhou, C.T. Chan, P. Sheng, Phys. Rev. Lett. 90 (2003) 083901.
[9] S.A. Ramakrishna, J.B. Pendry, M.C.K. Wiltshire, J. Mod. Opt. 50 (2003) 1419.
[10] S.A. Gredeskul, Y.S. Kivshar, A.A. Asatryan, K.Y. Bliokh, Y.P. Bliokh, V. D. Freilikher, I.V. Shadrivov, Low Temp. Phys. 38 (2012) 570.
[11] P. Markoš, R. Hlubina, unpublished.
[12] P.Y. Chen, et al., New J. Phys. 13 (2011) 053007.
[13] D. Hermann, et al., Phys. Rev. B 77 (2008) 035112.
[14] J.D. Joannopoulos, S.G. Johnson, J.N. Winnand, R.G. Meade, Photonic Crystals: Molding the Flow of Light, 2nd edition, Princeton University Press, Princeton, 2008.
[15] K. Sakoda, Optical Properties of Photonic Crystals, Springer, Heidelberg, Berlin, 2005.
[16] S. Fan, J.D. Joannopoulos, Phys. Rev. B 65 (2002) 235112.
[17] S. Fan, W. Suh, J.D. Joannopoulos, J. Opt. Soc. Am. A 20 (2003) 569.
[18] M.V. Rybin, K.B. Samusev, I.S. Sinev, G. Semouchkin, E. Semouchjina, Y. S. Kivshar, M.F. Limonov, Opt. Express 21 (2013) 30107.
[19] K. Ohtaka, H. Numata, Phys. Lett. 73A (1979) 411.
[20] A.A. Poddubny, et al., Nat. Commun. 3 (2012) 914.
[21] B. Lukyanchuk, et al., Nat. Mater. 9 (2010) 707.
[22] P. Markoš, Phys. Rev. A 92 (2015) 043814.
[23] J.A. Stratton, Electromagnetic Theory, Mc Graw-Hill Companies, New York, 1941.
[24] W.M. Robertson, et al., Phys. Rev. Lett. 68 (1992) 2023.
[25] C.A. Pfeiffer, E.N. Economou, K.L. Ngai, Phys. Rev. B 10 (1974) 3038.
[26] W.H. Press, et al., Numerical Recipes, Cambridge University Press, Cambridge, 1992.
[27] A.A. Asatryan, K.B. Dossou, L.C. Botten, Australian Institute of Physics, 18th National Congress, 2008.
[28] J.B. Pendry, et al., Phys. Rev. Lett. 76 (1996) 4773.
[29] P. Markoš, C.M. Soukoulis, Wave Propagation: From Electrons to Photons and Left-handed Materials, Princeton University Press, New Jersey, 2008.
[30] T. Vary, P. Markoš, Physica B 405 (2010) 2982.
[31] J.D. Jackson, Classical Electrodynamics, John Wiley and Sons, New York, 1999.
[32] M. Abramowitz, I.A. Stegun, Handbook of Mathematical Functions, Dover Publication Inc, New York, 1965.